

# High-brightness lasers on silicon by beam combining

Eric J. Stanton\*, Alexander Spott, Nicolas Volet, Michael L. Davenport, and John E. Bowers

Department of Electrical and Computer Engineering, University of California, Santa Barbara  
(UCSB), CA 93106, USA

## ABSTRACT

High-brightness lasers are widely used in fields such as spectroscopy, infrared countermeasures, free-space communication, and industrial manufacturing. Integration of a broad-band, multi-spectral laser is made possible by heterogeneously integrating multiple gain materials on one silicon (Si) substrate chip. A single multi-spectral output with high beam quality can be achieved by wavelength beam combining in multiple stages: within the gain bandwidth of each laser material and then coarsely combining each spectral band to a single output waveguide. To make power scaling feasible with this system, heterogeneously integrated lasers spanning the near- to the mid-infrared with corresponding low-loss wavelength beam combining elements on chip must be demonstrated. In this work, a review of multi-spectral lasers integrated on Si is presented and various waveguide materials are discussed for spanning the visible to the mid-infrared. Recent work integrating 2.0- $\mu\text{m}$  diode and 4.8- $\mu\text{m}$  quantum cascade lasers on Si extend the previously available 1.3- $\mu\text{m}$  and 1.5- $\mu\text{m}$  diode lasers on Si to the mid-infrared. Spectral beam combining elements for spanning the visible to the mid-infrared with low loss are discussed.

**Keywords:** Silicon photonics, wavelength division multiplexing, high-power lasers.

## 1. INTRODUCTION

For applications in manufacturing, remote sensing, medicine, military, and fundamental science an ideal laser would have high output power and a diffraction-limited beam. The figure-of-merit to describe this property is the brightness, which scales proportional to output power and inverse to the beam quality factor  $M^2$ . Lasers that are both compact and have high-brightness are challenging to realize. As the size of the laser is reduced, either the output power is decreased or the  $M^2$  is increased, primarily due to a combination of thermal effects and high optical intensities.<sup>1,2</sup> Many applications, such as spectroscopy, infrared countermeasures, free-space communication, and industrial manufacturing, benefit from the light source having multiple frequencies. A compact and high-brightness laser can then be achieved by spectral beam combining.<sup>3</sup> This photonic integrated circuit (PIC) may expand on the spectral bandwidth of currently available optical sources for less cost, smaller size, reduced vibration sensitivity, and higher brightness.

Over the past decade, advances in heterogeneous lasers on silicon (Si) enable such a multi-frequency and high-brightness laser to be integrated on a single cost-effective substrate.<sup>4,5</sup> With multiple die bonding,<sup>6,7</sup> materials exhibiting optical gain at various wavelengths are brought together onto a Si chip and lasers are formed with integrated mirrors. Outputs from each laser can be combined with various stages of wavelength division multiplexing optical elements,<sup>8</sup> as shown in Fig. 1. Semiconductor optical amplifiers (SOAs) are critical components for many kinds of photonic integrated circuits to increase output power or maintain signal levels as the signal propagates throughout a large number of optical components.<sup>9</sup> In our approach, SOAs are integrated on the same platform with the lasers on Si and, in addition to the concept of Fig. 1, could be used to increase power following each intra-band combiner.

This manuscript reviews recent progress on integration of multiple laser sources on a chip that combines the outputs to a single waveguide. Each laser gain material could support many lasers with densely spaced wavelengths, similar to modern optical communication systems filling the optical bandwidth of the erbium-doped-fiber-amplifier with densely-spaced frequency channels. To extend the spectral capacity of the Si-on-insulator (SOI) platform beyond the transmission window supported by a Si-core and silicon dioxide ( $\text{SiO}_2$ )-clad waveguide, a silicon nitride ( $\text{Si}_3\text{N}_4$ ) waveguide layer can be added.<sup>8</sup> Optical sources at 1.0- $\mu\text{m}$ ,<sup>18</sup> 1.3- $\mu\text{m}$ ,<sup>10</sup>

---

\*E-mail: estanton@ece.ucsb.edu

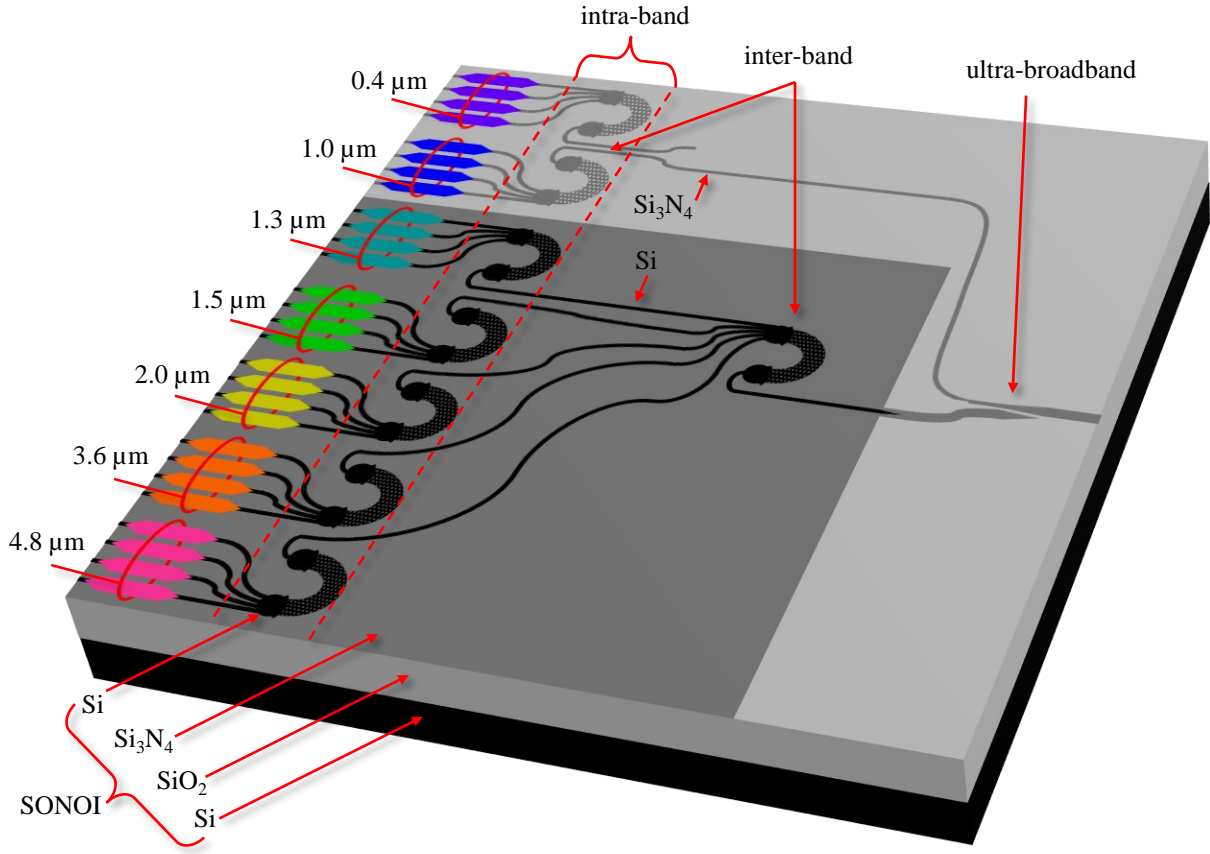


Figure 1. Schematic diagram of a multi-spectral laser on a Si substrate with the SONOI waveguide platform.

1.5- $\mu\text{m}$ ,<sup>4</sup> 2.0- $\mu\text{m}$ ,<sup>11</sup> and 4.8- $\mu\text{m}$ <sup>12</sup> wavelengths on Si have been demonstrated separately. Efficient integrated spectral combining elements have been investigated for coarse and dense wavelength combining stages.<sup>8</sup> In particular, efforts have been made to reduce the losses associated with arrayed waveguide gratings (AWGs) used in the dense wavelength combining stage. The following sections present the architecture for this multi-frequency high-brightness laser, discuss materials for broadband and low-loss operation, review demonstrations of lasers on Si with different wavelengths, and present integrated wavelength combining devices compatible with these lasers on Si.

## 2. ARCHITECTURE OF HIGH-BRIGHTNESS LASER

An ultra-broadband multi-spectral laser on Si is feasible with existing technology to heterogeneously integrate lasers on Si by direct wafer bonding.<sup>13,14</sup> This fully integrated device is schematized in Fig. 1, showing presently demonstrated spectral bands of lasers on Si at 1.3- $\mu\text{m}$ ,<sup>6,10</sup> 1.5- $\mu\text{m}$ ,<sup>4,9</sup> 2.0- $\mu\text{m}$ ,<sup>11,15</sup> and 4.8- $\mu\text{m}$ <sup>12,16</sup> wavelengths, based on indium phosphide (InP). Active devices have also been integrated with Si<sub>3</sub>N<sub>4</sub> at 1.0- $\mu\text{m}$ ,<sup>18</sup> based on gallium arsenide (GaAs), and at 1.5- $\mu\text{m}$ .<sup>17</sup> The spectral bands at 0.4- $\mu\text{m}$  and 3.6- $\mu\text{m}$  wavelengths will be realized with gallium nitride (GaN) and gallium antimonide (GaSb) based materials, respectively.

Spectral beam combining of each laser wavelength to a single output waveguide is achieved by several stages from dense to coarse wavelength division multiplexing (WDM). There is no inherent loss to combining. Note that AWGs efficiently combine light both for the dense WDM and for the coarse WDM with more than two channels. Adiabatic couplers can be designed to combine light for coarse WDM with just two inputs. Lasers with wavelengths longer than  $\sim 1.1 \mu\text{m}$  are integrated on Si waveguides, while shorter wavelength lasers are on Si<sub>3</sub>N<sub>4</sub> waveguides. The final ultra-broadband combining stage has been demonstrated<sup>8</sup> to combine light from

the visible (0.76  $\mu\text{m}$ ) to the mid-infrared (3.6  $\mu\text{m}$ ) with high fundamental mode transmission. Furthermore, simulations show efficient operation in the range of 0.35–6.7  $\mu\text{m}$ , however, this was not verified due to limited availability of optical sources. To obtain high brightness, every element of this PIC must be efficient. For the lasers, high wall-plug efficiency and output power are critical figures-of-merit. SOAs may also be included to boost the power of each spectral band. The beam combining elements must have low on-chip loss and transmit light to the fundamental modes of each wavelength in a single output waveguide.

The brightness ( $B$ ) is defined by the output power ( $P$ ) and the beam quality factor ( $M^2$ ) as:  $B = P/M^2$ . The transverse divergence angles ( $\theta_{\perp}$  and  $\theta_{\parallel}$ ) can be expressed from the diffraction-limited divergence angles ( $\theta_{\perp,0}$  and  $\theta_{\parallel,0}$ ) modified by the beam quality factors ( $M_{\perp}^2$  and  $M_{\parallel}^2$ ):  $\theta_{\perp} = \theta_{\perp,0}M_{\perp}^2$  and  $\theta_{\parallel} = \theta_{\parallel,0}M_{\parallel}^2$ . Both angles can be combined as:  $M^2 = (M_{\perp}^4 + M_{\parallel}^4)^{1/2}$ . The ideal condition of  $M^2 = 1.0$  is achieved by tailoring the output optical mode of the laser to have an exactly Gaussian-shaped intensity profile in the vertical and the horizontal orientations. For this reason, the passive beam-combining elements must transmit a high percentage of input light to the output fundamental mode. Additionally, the output waveguide must be able to support Gaussian-shaped modes throughout the bandwidth of the multi-spectral optical sources.

### 3. WAVEGUIDE MATERIAL PLATFORM

Investigation into waveguides for low-loss mid-infrared transmission has shown that Si can guide light from the near-infrared ( $\sim 1.1\text{-}\mu\text{m}$ ) to the mid-infrared ( $\sim 7.0\text{-}\mu\text{m}$ ) with low absorption loss.<sup>19, 20</sup>  $\text{SiO}_2$  and  $\text{Si}_3\text{N}_4$  are commonly integrated on Si and can be layered to create multiple waveguide cores in the same platform. These materials have transmission windows in the wavelength ranges of 0.35–3.5- $\mu\text{m}$  and 0.35–6.7- $\mu\text{m}$ , respectively.<sup>19, 20</sup> From this information, we have constructed a waveguide platform with layers of Si,  $\text{Si}_3\text{N}_4$ , and  $\text{SiO}_2$  on a Si substrate, called Si-on-nitride-on-insulator (SONOI)<sup>8, 12, 16</sup> and depicted in Fig. 1. By defining waveguides in the top Si layer and depositing an upper cladding of  $\text{Si}_3\text{N}_4$ , light from  $\sim 1.1\text{-}\mu\text{m}$  to  $\sim 6.7\text{-}\mu\text{m}$  wavelengths is efficiently guided. In other areas of the same chip, the top Si layer is removed and waveguides with  $\text{Si}_3\text{N}_4$  core and  $\text{SiO}_2$  cladding are defined to support  $\sim 0.4\text{-}\mu\text{m}$  to  $\sim 3.5\text{-}\mu\text{m}$  wavelengths. For longer wavelengths in the mid-infrared,  $\text{Si}_{1-x}\text{Ge}_x$  waveguides can transmit light with low-loss from 1.9- $\mu\text{m}$ , to 16.7- $\mu\text{m}$ .<sup>19, 21, 22</sup> This can potentially be integrated with the SONOI platform by adding the  $\text{Si}_{1-x}\text{Ge}_x$  on top of the Si waveguide layer.

### 4. LASERS HETEROGENEOUSLY INTEGRATED ON SILICON

In this section, the current spectral capabilities of heterogeneous lasers on Si are motivated and discussed. Fabrication for lasers and amplifiers at each spectral band follows a similar process, schematized in Fig. 2. More detailed processing information can be found in a recent manuscript about distributed feedback (DFB) lasers on Si.<sup>23</sup> Laser performance is reviewed at each wavelength and compared by the threshold currents, maximum output powers, and temperature dependencies.

#### 4.1 Lasers at 1.31- $\mu\text{m}$ on Si

One of the early demonstrations of the heterogeneously integrated laser operates at 1.31- $\mu\text{m}$  wavelength with an InP-based gain material.<sup>10</sup> A maximum output power of 32 mW is reported with a 35-mA threshold current at room temperature. Continuous-wave (CW) lasing up to 105 °C is observed. More recently, improved performance is shown with an 18-mA threshold current, 35-mW CW output power, and a wall-plug efficiency of 14 %.<sup>24</sup> The gain region length is only 700  $\mu\text{m}$  and higher output power is expected for a design with a longer gain region. Simultaneous operation of 16 lasers arrayed on the same chip is demonstrated. This spectral band has the most mature technology for fabrication and packaging.<sup>25</sup> Also, 1.31- $\mu\text{m}$  lasers are typically more efficient than 1.55- $\mu\text{m}$  lasers, because of lower intervalence band absorption<sup>26</sup> and reduced Auger recombination.<sup>27</sup>

#### 4.2 Lasers and SOAs at 1.55- $\mu\text{m}$ on Si

Since the first electrically pumped laser on Si was demonstrated,<sup>4</sup> there has been significant focus and development to improve performance and advance this technology for large scale integration to drive down the cost of optical communication systems. The most complex PICs using heterogeneous integration are at this wavelength.<sup>7</sup> A recent demonstration at 1.55- $\mu\text{m}$  details design optimization and performance for SOAs and lasers.<sup>9</sup>

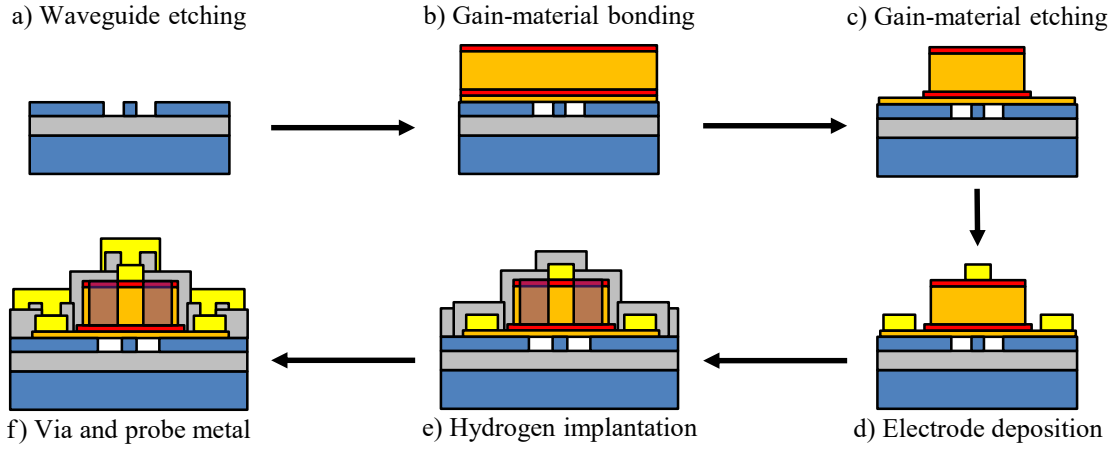


Figure 2. Fabrication steps (a–e) generalized for heterogeneously integrated lasers on Si, applicable to each spectral band discussed in Section 4. For some spectral bands (*i.e.*  $\sim 4.8\text{-}\mu\text{m}$ ), step (e) is skipped.

This work exemplifies a unique property of the heterogeneously integrated lasers and SOAs: the optical confinement is controlled lithographically by the Si waveguide width, independent of the current injection width or active region alterations. As a result, SOAs fabricated on the same chip may be designed with different values of gain and output saturation power. On-chip gain is demonstrated in the range 11–26 dB, as shown in Fig. 3(a), controlled by the Si waveguide width and corresponding to input saturation powers as high as 4 dBm. Operation over a wide bandwidth, plotted in Fig. 3(b), shows how a single SOA can amplify multi-spectral light following the intra-band combiner stage in Fig. 1.

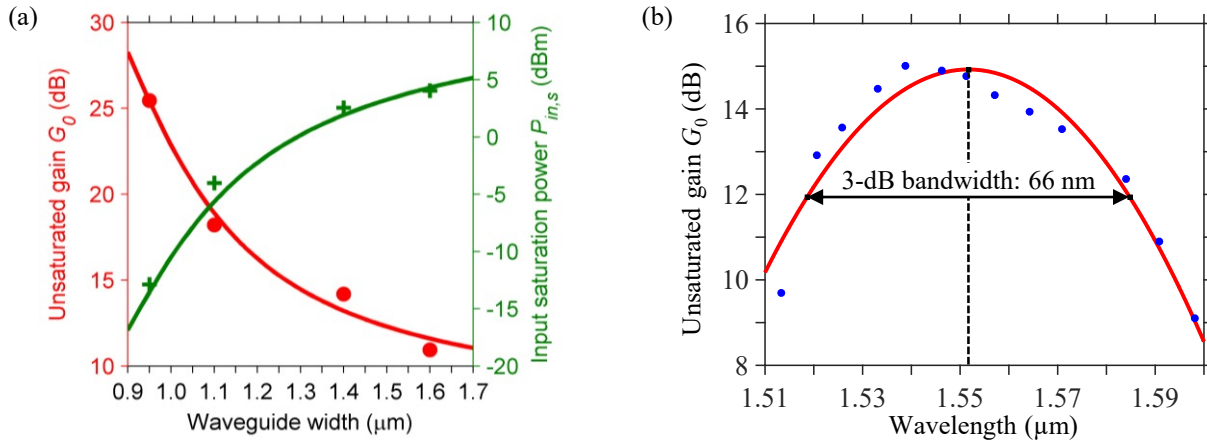


Figure 3. (a) Gain in the small-signal regime and input saturation power of an SOA operating at  $1.55\text{-}\mu\text{m}$  wavelength. (b) Gain extracted as a function of the wavelength. The fit (in red) shows the 3-dB bandwidth of the device.

Prior to the application of the anti-reflective (AR) coating to the SOAs, the devices lase from the Si-waveguide facet reflections, as schematized in Fig. 4(a). Output power is measured up to 42 mW, shown in Fig. 4(b). The thermal impedance is  $11\text{ K/W}$ ,<sup>9</sup> which is comparable to similar diodes on InP. Due to the high thermal conductivity of Si ( $1.56\text{ W}\cdot\text{cm}^{-1}\cdot\text{K}^{-1}$ ),<sup>28</sup> lateral heat spreading in the Si waveguide layer is responsible for this low thermal impedance. By defining a wide mesa of  $26\text{ }\mu\text{m}$ , the III-V is in contact with  $\sim 10\text{ }\mu\text{m}$  of the Si on both sides of the Si waveguide trench. Heat generated in the active region then has a low impedance path to this Si layer. Again, higher power is expected for longer gain region lengths.

A common challenge of heterogeneously integrated lasers is to produce an efficient optical mode converter

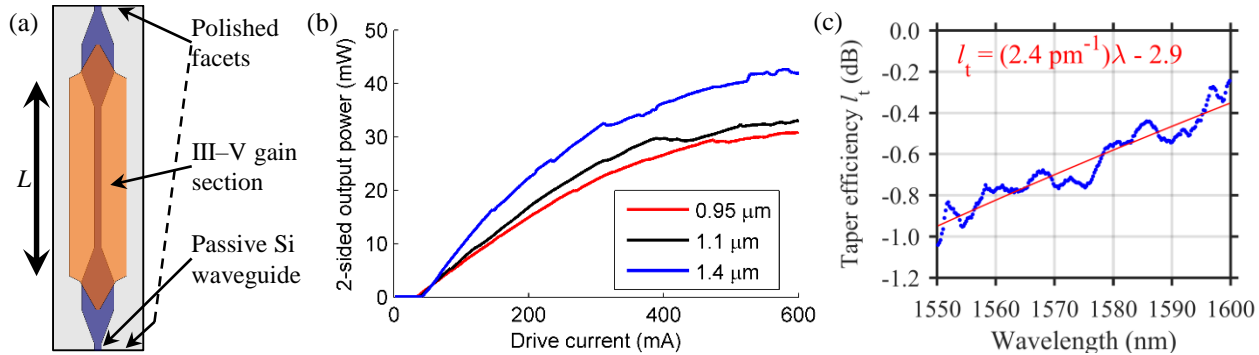


Figure 4. (a) Top-view schematic and (b) output power of a 1.55-μm laser. The polished Si-waveguide facets have a power reflection coefficient  $R = 0.28$  for each and define the laser cavity, which includes a gain section of length  $L = 2$  mm. (c) Extracted taper efficiency  $l_t$  versus the wavelength.

between the gain and the passive waveguide regions. This taper efficiency ( $l_t$ ), plotted in Fig. 4(c), has a maximum value of  $-0.25$  dB and increases as the wavelength increases. It is extracted from two similar lasers with different gain ( $g_1$  and  $g_2$ ), different gain-region lengths  $L_1$  and  $L_2$ , and a passive waveguide loss ( $\alpha_{\text{Si}} \approx 50$  dB/m) as:

$$l_t \equiv \frac{L_1 g_2 - L_2 g_1}{2(L_2 - L_1)} - \alpha_{\text{Si}} L_2. \quad (1)$$

Note that this relation depends on the wavelength and the current density. By accurately characterizing the taper loss, designs can be optimized for lasers at each wavelength for the multi-spectral laser described in Sect. 2.

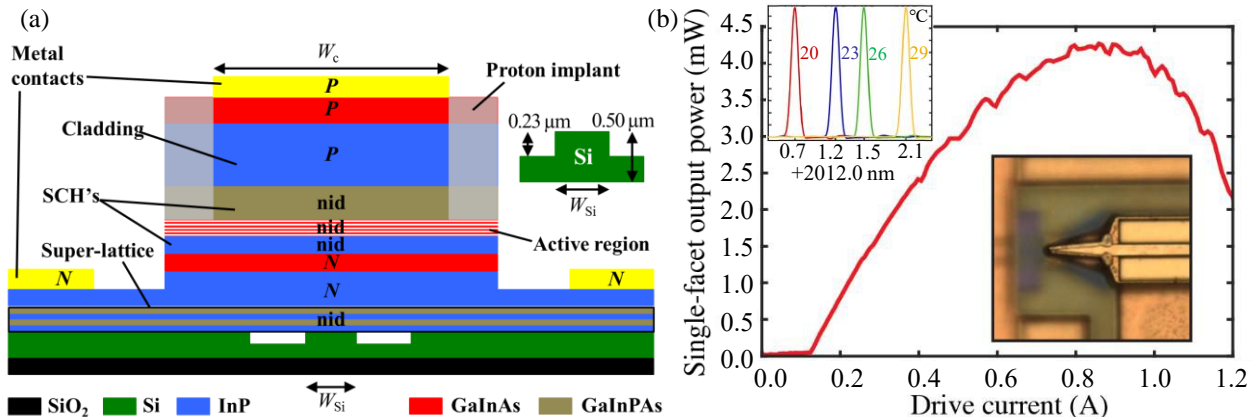


Figure 5. (a) Cross-section schematic of 2.0-μm laser or SOA on Si. (b) Output power characteristic with insets showing the laser spectra at different temperatures and a micrograph of the taper transition between the gain and passive regions.

### 4.3 Lasers and SOAs at 2.0-μm on Si

Si exhibits both a low two-photon absorption coefficient and a high Kerr coefficient at  $\sim 2.0$ -μm wavelength.<sup>29</sup> Therefore, low waveguide propagation loss is expected in this spectral band. Also, Si provides a power-efficient platform for chip-level applications in non-linear optics,<sup>30–32</sup> including comb generation and on-chip doubling,<sup>33</sup> so PICs with integrated 2.0-μm active devices are highly desired.

Recently, the first laser operating at 2-μm wavelength on Si was demonstrated.<sup>11</sup> The first ever reported 2-μm SOA was also demonstrated on Si.<sup>15</sup> These devices consist of GaInAs quantum wells (QWs) bonded on top of a Si waveguide. A cross-section schematic is drawn in Fig. 5(a). The hybrid optical mode is laterally confined by the Si waveguide, while a portion of the mode overlaps the active region. The III–V mesa is terminated on

both sides by a lateral taper, causing the hybrid active mode to couple into a passive Si waveguide mode. A Fabry–Perot cavity is then formed by the polished Si facets for the lasers, and they are AR coated to form the SOAs. The laser output power, plotted in Fig. 5(b), has emission up to 4.2 mW from a single facet with a  $\sim$ 122-mA threshold current. CW lasing is observed up to 35 °C. The SOA on-chip gain has current and wavelength

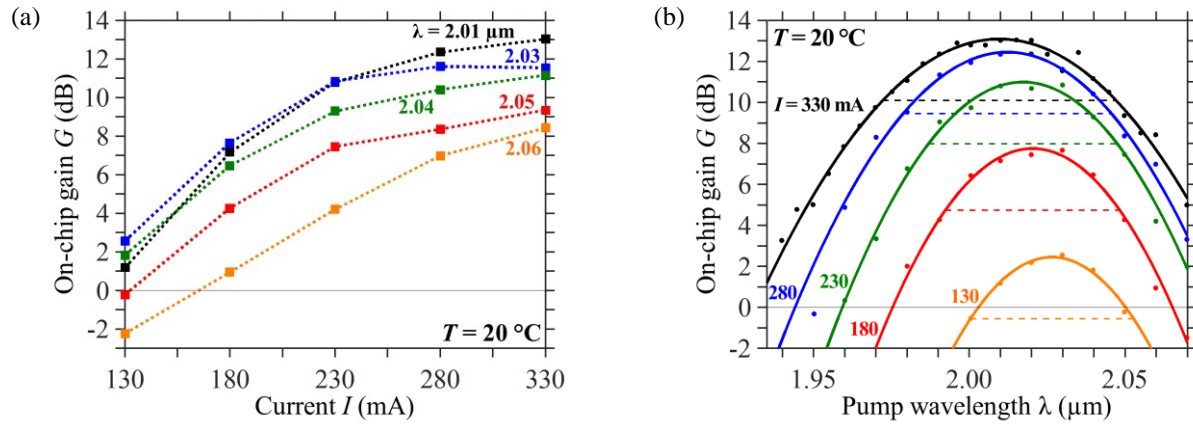


Figure 6. (a) Schematic of taper loss test structures. (b) Extracted taper loss  $l_t$  wavelength dependence.

dependencies as plotted in Fig. 6. A maximum gain of 13-dB is observed and gain is demonstrated up to 50 °C.

#### 4.4 Lasers at 4.8- $\mu\text{m}$ on Si

Light of longer wavelengths than 3  $\mu\text{m}$  can be exploited for numerous sensing and detection applications. Chemical bond spectroscopy,<sup>34</sup> environmental monitoring, and remote sensing<sup>35</sup> can potentially be addressed on an integrated Si platform. Low-cost, versatile, and complex technologies can be enabled by integrating multiple sensors on one Si chip. However, room-temperature InP-based type-I diode lasers have only been reported up to  $\sim$ 2.4  $\mu\text{m}$ .<sup>36</sup> Alternatively, GaSb-based interband cascade lasers (ICL) and InP-based quantum cascade lasers (QCL) are promising candidates for extending heterogeneous integration to wavelengths throughout the mid-infrared (3.0–8.0  $\mu\text{m}$ ). QCLs operate from 3.0  $\mu\text{m}$  to the terahertz regime and can emit watts of CW output power.<sup>37,38</sup>

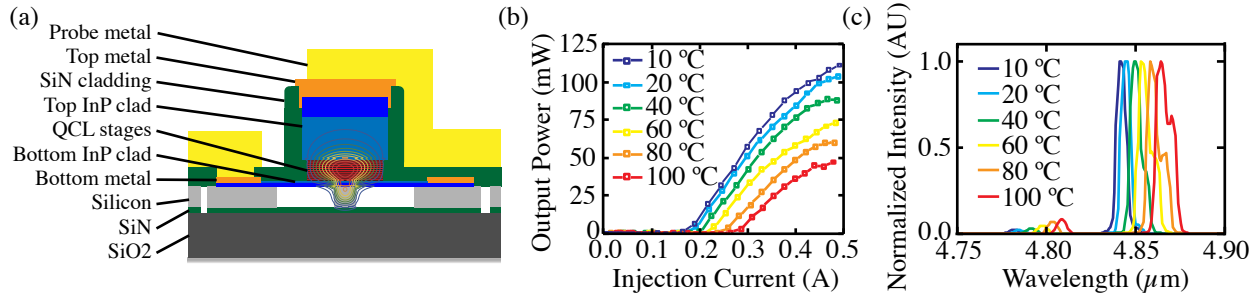


Figure 7. (a) Schematic of QCL on Si. (b) Output power of Si–QCL (pulsed) as a function of current and temperature. (c) Normalized emission spectra temperature dependence.

Last year, the first QCLs integrated on Si were demonstrated with operation at a wavelength near 4.8  $\mu\text{m}$ .<sup>12</sup> These lasers utilize a III–V active mesa bonded to Si and tapered at both ends to transfer light into passive Si waveguides. A cross-sectional schematic of the active region of a heterogeneously integrated QCL is shown in Fig. 7(a). Due to the high material absorption of SiO<sub>2</sub>, the traditionally-used SOI platform is not ideal for

mid-infrared Si photonic integration. The QCLs are therefore integrated on the SONOI waveguide platform, which should permit transmission of the wavelength range 1.1–6.7  $\mu\text{m}$ .

The first integrated QCLs include a Fabry–Perot laser cavity, operated in pulsed mode at room temperature, and exhibit threshold currents as low as 387 mA and output powers up to 31 mW per facet. Subsequent advancements are demonstrated with DFB lasers, which employ a  $\lambda/4$ -shifted grating on top of Si waveguides within the active region.<sup>16</sup> These wavelength-selective devices emit over 200 mW from a single facet after removing the III–V taper. This verifies that high power and low threshold QCLs can be integrated on Si with improved taper design. In Fig. 7(b) the light output versus drive current for an integrated DFB QCL is shown operating at temperatures from 10 °C to 100 °C. These results open the opportunity to build a wide range of fully-integrated sensors and detectors on Si operating with wavelengths throughout the mid-infrared.

## 5. INTEGRATED SPECTRAL BEAM COMBINING

This section describes the passive wavelength beam combining devices for integration with the different lasers discussed in Section 4. In particular, devices for dense and coarse WDM are reviewed to present how the intra-band, inter-band, and ultra-broadband stages in Fig. 1 are realized.

### 5.1 Dense WDM

For the range of wavelengths generated from a single gain material, a dense WDM device will combine each laser output to a single waveguide. AWGs provide the most efficient spectral beam combining for dense spectral spacing. Measurement results for AWGs operating near 0.76- $\mu\text{m}$ , 1.55- $\mu\text{m}$ , and 2.0- $\mu\text{m}$  wavelengths are reviewed and a recently fabricated AWG at 3.6- $\mu\text{m}$  is shown in this sub-section.

Low-loss AWGs are achieved by minimizing loss contributions from waveguide propagation, width transitions, and bend radius transitions. Phase errors in the arrayed waveguides must also be minimized. Additionally, the waveguide array in the AWG must have low side-order excitation. All of these design aspects become more problematic for shorter wavelengths compared AWGs commonly made in the near-infrared for communication applications. For bulk material, Rayleigh scattering dominates, which is proportional to  $\lambda^{-4}$ ,<sup>39</sup> and for waveguides, interfacial scattering dominates, having a similar wavelength dependence.<sup>40,41</sup> Phase errors arise due to lithography inaccuracies (from mask writing or photoresist exposure), waveguide interfacial roughness, or non-uniformities in the waveguide thickness and in the etch. These fabrication-related limitations have greater effect at reduced wavelengths.

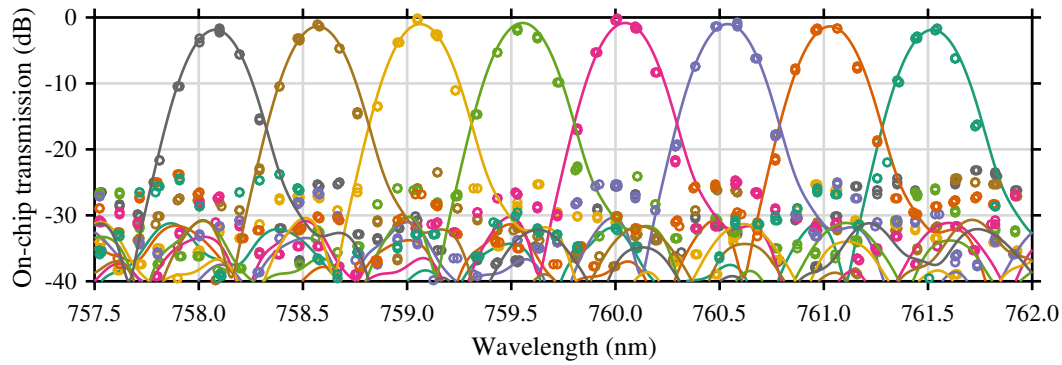


Figure 8. Transmission spectra for the 8 channels of an AWG at 0.76- $\mu\text{m}$  wavelength. Dots show the experimental data and the solid lines are simulations.

To optimize our design tools, an AWG near 0.76- $\mu\text{m}$  wavelength is demonstrated<sup>42</sup> before attempting longer wavelength AWGs. The waveguide core is  $\text{Si}_3\text{N}_4$  and cladding is  $\text{SiO}_2$ , consistent with the SONOI platform. A record low loss of <0.5 dB and crosstalk level of –25 dB is reported. The on-chip transmission data and model are plotted in Fig. 8, which show good agreement within the ~20-dB peak channel bandwidths. However, the

crosstalk level of the model is about 5 dB lower than the data. This is attributed to fabrication variations, such as waveguide thickness and etch non-uniformities, that are not included in the model.

Recently, AWGs near 1.55- $\mu\text{m}$  and 2.0- $\mu\text{m}$  wavelengths have been demonstrated on SOI with eight channels. The 1.55- $\mu\text{m}$  AWG is reported with <1.6 dB of loss and about -29 dB of crosstalk.<sup>43</sup> Preliminary measurements of the 2.0- $\mu\text{m}$  AWG reveals a low loss of <1.0 dB and crosstalk at about -28 dB, shown in Fig. 9. Also, a

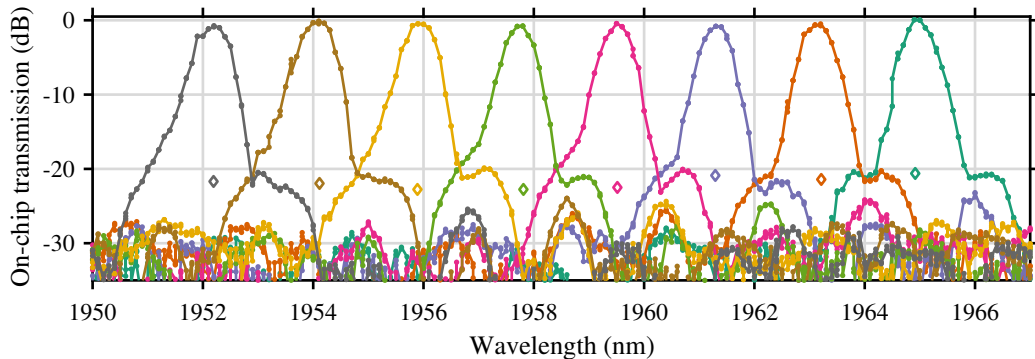


Figure 9. Transmission spectra for 8 channels of an AWG at 2.0- $\mu\text{m}$  wavelength. Diamonds show the 3-dB bandwidth cumulative crosstalk.

3.6- $\mu\text{m}$  wavelength AWG has been designed on SOI and the simulated performance is shown in Fig. 10(a) with a micrograph of the device in Fig. 10(b). Future work will compare the performance of these AWG demonstrations on SOI to similar designs on SONOI. This will indicate if loss decreases with SONOI due to the reduced material absorption of  $\text{Si}_3\text{N}_4$  compared to  $\text{SiO}_2$  or if excess loss arises from the additional material interfaces.

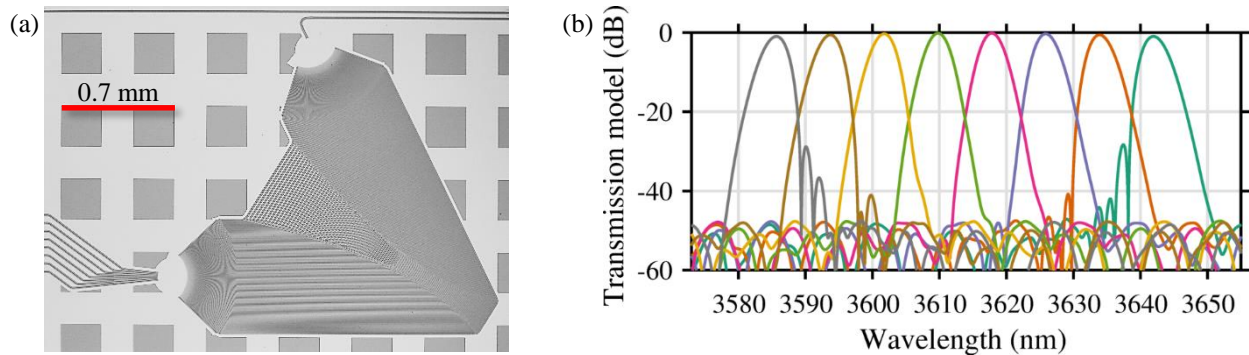


Figure 10. (a) Micrograph of a 3.6- $\mu\text{m}$  AWG. (b) Simulated transmission spectra for 8 channels of the AWG.

## 5.2 Coarse WDM

Inter-band combiners are either realized with adiabatic couplers or AWGs. The adiabatic coupler serves as a wavelength combiner with two inputs and one output, operating over spectral ranges spanning multiple octaves. These duplexers can achieve very low loss, only limited by the waveguide propagation loss (<0.05 dB). AWGs can combine more spectral channels, however, the loss is higher ( $\sim$ 1.0 dB) and the bandwidth is narrower.

The final combiner stage must be *ultra*-broadband, guiding and combining wavelengths that span more than four octaves to converge the each laser output into a single waveguide. For the applications mentioned in Sect. 1, the efficiency of fundamental mode excitation at each wavelength is important because this determines the output beam quality and affects the brightness ( $B$ ) of the multi-spectral laser. A modified adiabatic coupler has been demonstrated to meet these specifications.<sup>8</sup> One input to this combiner supports the short wavelengths and the other the long wavelengths. A narrow spectral region near 1.55- $\mu\text{m}$  exhibits decreased transmission with a

maximum loss of 3.0 dB. Less than 0.5-dB loss is found between 0.35- $\mu$ m to 1.3- $\mu$ m for one input and 1.9- $\mu$ m to 6.5- $\mu$ m light for the other. The center of the low-transmission region can be tuned by changing the length of the coupler, which is independent of the operating bandwidth.

## 6. CONCLUSION AND PROSPECTIVES

Each element of the high-brightness multi-spectral laser on silicon has been demonstrated and a path towards complete integration is feasible. High powered lasers spanning the near-infrared to the mid-infrared are integrated on silicon. Low-loss beam combining elements are realized at corresponding wavelengths to the optical sources, paving the way for full-system integration. Remaining challenges for this multi-spectral PIC are to improve laser wall-plug efficiencies and to develop a fabrication process for simultaneous integration of InP with other gain materials. This technology is important to enable fully-integrated multi-spectral lasers for highly attuned gas sensors, infrared counter-measures, ultra-broadband WDM optical communications, and industrial processing. Fabrication of this device is scalable and would drastically reduce the cost compared to technologies with similar performance.

## ACKNOWLEDGMENTS

This research is funded by the Air Force Research Laboratory (AFRL), contract FA8650-17-C-5402, and the Office of Naval Research (ONR), contract N00014-13-C-0147. N.V. is supported by the Swiss National Science Foundation.

## REFERENCES

- [1] Siegman, A., "Analysis of laser beam quality degradation caused by quartic phase aberrations," *Appl. Opt.* **32**(30), 5893–5901 (1993).
- [2] Paschotta, R., "Beam quality deterioration of lasers caused by intracavity beam distortions," *Opt. Express* **14**(13), 6069–6074 (2006).
- [3] Fan, T. Y., "Laser beam combining for high-power, high-radiance sources," *IEEE J. Sel. Topics Quantum Electron.* **11**(3), 567–577 (2005).
- [4] Fang, A. W., Park, H., Cohen, O., Jones, R., Paniccia, M. J., and Bowers, J. E., "Electrically pumped hybrid AlGaInAs-silicon evanescent laser," *Opt. Express* **14**(20), 9203–9210 (2006).
- [5] Liang, D. and Bowers, J. E., "Recent progress in lasers on silicon," *Nat. Phot.* **4**(8), 511–517 (2010).
- [6] Chang, H.-H., Kuo, Y.-h., Jones, R., Barkai, A., and Bowers, J. E., "Integrated hybrid silicon triplexer," *Opt. Express* **18**(23), 23891–23899 (2010).
- [7] Zhang, C., Zhang, S., Peters, J. D., and Bowers, J. E., "8×8×40 Gbps fully integrated silicon photonic network on chip," *Optica* **3**(7), 785–786 (2016).
- [8] Stanton, E. J., Heck, M. J. R., Bovington, J., Spott, A., and Bowers, J. E., "Multi-octave spectral beam combiner on ultra-broadband photonic integrated circuit platform," *Opt. Express* **23**(9), 11272–11283 (2015).
- [9] Davenport, M. L., Skendžić, S., Volet, N., Hulme, J. C., Heck, M. J., and Bowers, J. E., "Heterogeneous Silicon/III-V Semiconductor Optical Amplifiers," *IEEE J. Sel. Topics Quantum Electron.* **22**(6), 78–88 (2016).
- [10] Chang, H.-H., Fang, A. W., Sysak, M. N., Park, H., Jones, R., Cohen, O., Raday, O., Paniccia, M. J., and Bowers, J. E., "1310nm silicon evanescent laser," *Opt. Express* **15**(18), 11466–11471 (2007).
- [11] Spott, A., Davenport, M., Peters, J., Bovington, J., Heck, M. J., Stanton, E. J., Vurgaftman, I., Meyer, J., and Bowers, J., "Heterogeneously integrated 2.0  $\mu$ m cw hybrid silicon lasers at room temperature," *Opt. Lett.* **40**(7), 1480–1483 (2015).
- [12] Spott, A., Peters, J., Davenport, M. L., Stanton, E. J., Merritt, C. D., Bewley, W. W., Vurgaftman, I., Kim, C. S., Meyer, J. R., Kirch, J., et al., "Quantum cascade laser on silicon," *Optica* **3**(5), 545–551 (2016).
- [13] Liang, D., Fang, A. W., Park, H., Reynolds, T. E., Warner, K., Oakley, D. C., and Bowers, J. E., "Low-Temperature, Strong SiO<sub>2</sub>-SiO<sub>2</sub> Covalent Wafer Bonding for III-V Compound Semiconductors-to-Silicon Photonic Integrated Circuits," *J. of Electron. Mater.* **37**(10), 1552–1559 (2008).

- [14] Liang, D., Chapman, D. C., Li, Y., Oakley, D. C., Napoleone, T., Juodawlkis, P. W., Brubaker, C., Mann, C., Bar, H., Raday, O., et al., "Uniformity study of wafer-scale InP-to-silicon hybrid integration," *Appl. Phys. A Mater. Sci. Process.* **103**(1), 213–218 (2011).
- [15] Volet, N., Spott, A., Stanton, E. J., Davenport, M. L., Chang, L., Peters, J. D., Briles, T. C., Vurgaftman, I., Meyer, J. R., and Bowers, J. E., "Semiconductor optical amplifier at 2.0- $\mu\text{m}$  wavelength on silicon," *Laser Photon. Rev.* (accepted in January 2017).
- [16] Spott, A., Peters, J., Davenport, M. L., Stanton, E. J., Zhang, C., Merritt, C. D., Bewley, W. W., Vurgaftman, I., Kim, C. S., Meyer, J. R., Kirch, J., Mawst, L. J., Botez, D., and Bowers, J. E., "Heterogeneously Integrated Distributed Feedback Quantum Cascade Lasers on Silicon," *Photonics* **3**(2), 35 (2016).
- [17] Piels, M., Bauters, J. F., Davenport, M. L., Heck, M. J., and Bowers, J. E., "Low-loss silicon nitride AWG de-multiplexer heterogeneously integrated with hybrid III-V/silicon photodetectors," *J. Lightw. Technol.* **32**(4), 817–823 (2014).
- [18] Bovington, J., Heck, M., and Bowers, J., "Heterogeneous lasers and coupling to  $\text{Si}_3\text{N}_4$  near 1060 nm," *Opt. Lett.* **39**(20), 6017–6020 (2014).
- [19] Soref, R. A., Emelett, S. J., and Buchwald, W. R., "Silicon waveguided components for the long-wave infrared region," *J. Opt. A: Pure Appl. Opt.* **8**(10), 840–846 (2006).
- [20] Soref, R., "Mid-infrared photonics in silicon and germanium," *Nat. Photon.* **4**(8), 495–497 (2010).
- [21] Li, W., Anantha, P., Bao, S., Lee, K. H., Guo, X., Hu, T., Zhang, L., Wang, H., Soref, R., and Tan, C. S., "Germanium-on-silicon nitride waveguides for mid-infrared integrated photonics," *Appl. Phys. Lett.* **109**(24), 241101 (2016).
- [22] Ramirez, J. M., Vakarin, V., Gilles, C., Frigerio, J., Ballabio, A., Chaisakul, P., Le Roux, X., Alonso-Ramos, C., Maisons, G., Vivien, L., et al., "Low-loss Ge-rich  $\text{Si}_{0.2}\text{Ge}_{0.8}$  waveguides for mid-infrared photonics," *Opt. Lett.* **42**(1), 105–108 (2017).
- [23] Zhang, C., Srinivasan, S., Tang, Y., Heck, M. J., Davenport, M. L., and Bowers, J. E., "Low threshold and high speed short cavity distributed feedback hybrid silicon lasers," *Opt. Express* **22**(9), 10202–10209 (2014).
- [24] Koch, B. R., Norberg, E. J., Kim, B., Hutchinson, J., Shin, J.-H., Fish, G., and Fang, A., "Integrated silicon photonic laser sources for telecom and datacom," in [National Fiber Optic Engineers Conference], Paper PDP5C-8, OSA (2013).
- [25] Liu, H.-F., "Integrated silicon photonics links for high bandwidth data transportation," in [Optical Fiber Communication Conference], Paper Th1D.1, OSA (2014).
- [26] Casey Jr., H. C. and Carter, P. L., "Variation of intervalence band absorption with hole concentration in *p*-type InP," *Appl. Phys. Lett.* **44**(1), 82–83 (1984).
- [27] Volet, N. and Kapon, E., "Turn-on delay and Auger recombination in long-wavelength vertical-cavity surface-emitting lasers," *Appl. Phys. Lett.* **97**(13), 131102 (2010).
- [28] Glassbrenner, C. and Slack, G. A., "Thermal conductivity of silicon and germanium from 3°K to the melting point," *Phys. Rev.* **134**(4A), A1058 (1964).
- [29] Bristow, A. D., Rotenberg, N., and van Driel, H. M., "Two-photon absorption and Kerr coefficients of silicon for 850–2200 nm," *Appl. Phys. Lett.* **90**(19), 191104 (2007).
- [30] Foster, M. A., Turner, A. C., Sharping, J. E., Schmidt, B. S., Lipson, M., and Gaeta, A. L., "Broad-band optical parametric gain on a silicon photonic chip," *Nature* **441**(7096), 960–963 (2006).
- [31] Zlatanovic, S., Park, J. S., Moro, S., Boggio, J. M. C., Divlansky, I. B., Alic, N., Mookherjea, S., and Radic, S., "Mid-infrared wavelength conversion in silicon waveguides using ultracompact telecom-band-derived pump source," *Nat. Photon.* **4**(8), 561–564 (2010).
- [32] Del'Haye, P., Herr, T., Gavartin, E., Gorodetsky, M., Holzwarth, R., and Kippenberg, T. J., "Octave spanning tunable frequency comb from a microresonator," *Phys. Rev. Lett.* **107**(6), 063901 (2011).
- [33] Chang, L., Li, Y., Volet, N., Wang, L., Peters, J., and Bowers, J. E., "Thin film wavelength converters for photonic integrated circuits," *Optica* **3**(5), 531–535 (2016).

- [34] Rothman, L. S., Gordon, I. E., Babikov, Y., Barbe, A., Benner, D. C., Bernath, P. F., Birk, M., Bizzocchi, L., Boudon, V., Brown, L. R., Campargue, A., Chance, K., Cohen, E. A., Coudert, L. H., Devi, V. M., Drouin, B. J., Fayt, A., Flaud, J.-M., Gamache, R. R., Harrison, J. J., Hartmann, J.-M., Hill, C., Hodges, J. T., Jacquemart, D., Jolly, A., Lamouroux, J., Roy, R. J. L., Li, G., Long, D. A., Lyulin, O. M., Mackie, C. J., Massie, S. T., Mikhailenko, S., Muller, H. S. P., Naumenko, O. V., Nikitin, A. V., Orphal, J., Perevalov, V., Perrin, A., Polovtseva, E. R., Richard, C., Smith, M. A. H., Starikova, E., Sung, K., Tashkun, S., Tennyson, J., Toon, G. C., Tyuterev, V. G., and Wagner, G., "The HITRAN2012 molecular spectroscopic database," *J. Quant. Spectrosc. Radiat. Transfer* **130**, 4–50 (2013).
- [35] Salisbury, J. W. and D'Aria, D. M., "Emissivity of terrestrial materials in the 3–5  $\mu\text{m}$  atmospheric window," *Remote Sens. Environ.* **47**(3), 345–361 (1994).
- [36] Gu, Y., Zhang, Y., Cao, Y., Zhou, L., Chen, X., Li, H., and Xi, S., "2.4  $\mu\text{m}$  InP-based antimony-free triangular quantum well lasers in continuous-wave operation above room temperature," *Appl. Phys. Express* **7**(3), 032701 (2014).
- [37] Bai, Y., Bandyopadhyay, N., Tsao, S., Slivken, S., and Razeghi, M., "Room temperature quantum cascade lasers with 27% wall plug efficiency," *Appl. Phys. Lett.* **98**(18), 181102 (2011).
- [38] Yao, Y., Hoffman, A. J., and Gmachl, C. F., "Mid-infrared quantum cascade lasers," *Nat. Photon.* **6**(7), 432–439 (2012).
- [39] Strutt, J. W., "On the light from the sky, its polarization and colour," *Philos. Mag.* **41**(271), 107–120 (1871).
- [40] Bauters, J. F., Heck, M. J., John, D. D., Barton, J. S., Bruinink, C. M., Leinse, A., Heideman, R. G., Blumenthal, D. J., and Bowers, J. E., "Planar waveguides with less than 0.1 dB/m propagation loss fabricated with wafer bonding," *Opt. Express* **19**(24), 24090–24101 (2011).
- [41] Barwicz, T. and Haus, H. A., "Three-dimensional analysis of scattering losses due to sidewall roughness in microphotonic waveguides," *J. Lightw. Technol.* **23**(9), 2719 (2005).
- [42] Stanton, E. J., Spott, A., Davenport, M. L., Volet, N., and Bowers, J. E., "Low-loss arrayed waveguide grating at 760 nm," *Opt. Lett.* **41**(8), 1785–1788 (2016).
- [43] Stanton, E. J., Volet, N., and Bowers, J. E., "Ring resonator with cascaded arrayed waveguide gratings for accurate insertion loss measurement," in [IEEE Photonics Conference (IPC)], Paper MB3.4 (2016).